



This is a repository copy of *Adaptive beamforming for target detection and surveillance based on distributed unmanned aerial vehicle platforms*.

White Rose Research Online URL for this paper:

<https://eprints.whiterose.ac.uk/138012/>

Version: Published Version

---

**Article:**

Shen, Q., Liu, W. orcid.org/0000-0003-2968-2888, Wang, L. et al. (1 more author) (2018) Adaptive beamforming for target detection and surveillance based on distributed unmanned aerial vehicle platforms. *IEEE Access*, 6. pp. 60812-60823. ISSN 2169-3536

<https://doi.org/10.1109/ACCESS.2018.2875560>

---

**Reuse**

This article is distributed under the terms of the Creative Commons Attribution (CC BY) licence. This licence allows you to distribute, remix, tweak, and build upon the work, even commercially, as long as you credit the authors for the original work. More information and the full terms of the licence here:  
<https://creativecommons.org/licenses/>

**Takedown**

If you consider content in White Rose Research Online to be in breach of UK law, please notify us by emailing [eprints@whiterose.ac.uk](mailto:eprints@whiterose.ac.uk) including the URL of the record and the reason for the withdrawal request.

# Adaptive Beamforming for Target Detection and Surveillance Based on Distributed Unmanned Aerial Vehicle Platforms

Qing Shen, Wei Liu\*, Senior Member, IEEE, Li Wang\*, and Yin Liu

**Abstract**—A distributed sensor array network for target detection and surveillance is studied with sub-arrays placed on unmanned aerial vehicle (UAV) platforms, where arbitrary locations and rotation angles are allocated to each UAV-based sub-array in the predefined Cartesian coordinate system. In this model, one transmitter sends out a single signal and it is then reflected back from the targets and received by the distributed sensor array system. A joint reference signal based beamformer (JRSB) is proposed for the static/slowly moving targets and UAV platforms where the Doppler effects can be ignored, leading to improved performance by exploiting the information collected by all the sub-arrays simultaneously. Then, the developed beamformer is extended to the dynamic case considering the Doppler effects, referred to as the frequency extended joint reference signal based beamformer (FE-JRSB), achieving the potential maximum output signal to interference plus noise ratio (SINR) by exploiting the information across the potential frequencies of interest jointly. The output signal of the beamformer with increased SINR can be used to assist the extended target detection in the following processing. Simulation results show that both are able to extract the signals of interest while suppressing interfering signals, and a lower mean square error and higher output SINR are achieved compared with a regular reference signal based beamformer using a single sub-array. One unique feature of the provided solutions is that, although the signals involved are narrowband, the employed beamforming structure has to be wideband for it to be effective.

**Index Terms**—Adaptive beamforming, distributed sensor network, unmanned aerial vehicle, static/moving targets, Doppler frequency.

## I. INTRODUCTION

With the purpose of enhancing the received signals of interest (SOI) from certain directions while suppressing the interfering signals from other directions in a data-dependent manner, adaptive beamforming has been studied over the decades due to its extensive applications in wireless communications, radar, sonar, navigation, medical diagnosis, speech enhancement, and so on [1]–[4].

The linearly constrained minimum variance (LCMV) beamformer and the reference signal based (RSB) beamformer are two classes of well known beamformers [5]–[8]. For the

LCMV beamformer, the direction of arrival (DOA) information of the signal of interest is known or can be estimated in advance. By imposing several linear constraints to the minimization problem of the output variance, the LCMV beamformer and their extensions [9], [10] offer improved robustness against inaccurate DOA estimates as well as sensor position errors and other advantages such as flexible sidelobe control. On the other hand, a reference signal is assumed to be available for the RSB beamformer [11], [12], where adaptive beamforming is achieved by minimizing the mean square error (MSE) between the reference signal and the beamformer output. Most of the adaptive algorithms for both beamformers are derived based on some stochastic gradient (SG) methods [13], and many variations and extensions in the wideband case have been proposed [14]–[18].

In active sensing applications for target detection and parameter estimation, digital beamforming is applied to phased-array radars and adaptive radars [19], [20] to maximize the signal to noise plus interference ratio (SINR). Space-time adaptive processing (STAP) [21]–[23] is proposed for moving target indication against strong interference background through spatial (or space-time) beamforming, and it is commonly used for airborne radars.

Traditionally, the aforementioned beamformers are based on a single array with its sensors considered as part of a whole centred system, and distributed sensor arrays based on multi-static platforms have attracted increasing attention in recent years. For example, distributed microphone arrays are employed to extract spatial information for acoustic scene analysis [24], and multistatic radar systems [25], [26] are utilized for target detection and localization. However, a multistatic radar system consists of independent radars performing local processing, with a central processor fusing these information to form a final decision instead of coherent accumulation across all signals collected by independent radars simultaneously. The MIMO radar with widely separated antennas [26], [27] is employed for target detection and tracking with improved performance by exploiting radar cross section (RCS) spatial diversity.

Therefore, in this paper, a distributed sensor array network for target detection and surveillance with sub-arrays based on unmanned aerial vehicle (UAV) platforms is studied, where the sub-array on each UAV may have an arbitrary rotation angle in the predefined Cartesian coordinate system, which results in different impinging angles for different UAVs. For such a distributed sensor array system, it is necessary to enhance the

\*Corresponding authors: W. Liu and L. Wang.

Q. Shen and W. Liu are with the Department of Electronic and Electrical Engineering, University of Sheffield, Sheffield, S1 3JD, UK, and Q. Shen is also with the School of Information and Electronics, Beijing Institute of Technology, Beijing, 100081, China (e-mail: qing-shen@outlook.com, w.liu@sheffield.ac.uk).

L. Wang and Y. Liu are with the 10th Research Institute of China Electronics Technology Group Corporation.

received signals of interest for this kind of resource-limited (in terms of energy consumption, weight, and size) distributed UAV platforms via exploiting information acquired by all distributed sub-arrays simultaneously, so that an extended detection range and accuracy can be achieved. Since the sub-array based UAV platforms may have unknown positions, velocities, moving directions, and rotation angles, this is an extremely challenging problem.

In this studied scenario, one transmitter sends out a known signal and it is then reflected back from the target and received by the distributed sensor array system. The known transmitted signal can be considered as a reference signal. Based on this model, first we consider the case with static or slowly moving targets and UAV platforms, where the Doppler effect can be ignored, and a joint reference signal based beamformer (JRSB) is proposed to exploit the information acquired by all sub-arrays simultaneously, leading to improved performance compared with that of a regular RSB applied to a single UAV. Due to the extremely large spacing among the UAV platforms compared to half wavelength at the working frequency, signals received at different sub-arrays should not be considered as narrowband any more and a wideband beamforming structure should be employed instead [15], [16].

Then, we consider a dynamic case with moving targets and UAV platforms, where the Doppler effect cannot be ignored. To perform beamforming without prior knowledge of the motion parameters of both the targets and the UAV platforms, the JRSB is further extended as a solution by modulating the received signals into different frequency bins in the first step, referred to as the frequency extended joint reference signal based beamformer (FE-JRSB), to exploit the information across the frequencies of interest jointly. The potential maximum output SINR can be achieved by the FE-JRSB without sacrificing any information, and the output signal of the beamformer with increased SINR can be used for extended target detection in the following processing.

This paper is structured as follows. The distributed sensor array network consisting of different sub-arrays carried by UAV platforms is presented in Section II. The developed joint reference signal based beamformer (JRSB) for static (or slowly moving) targets and UAV platforms is proposed in Section III, and the frequency extended joint reference signal based beamformer (FE-JRSB) for the dynamic case is proposed in Section IV. Simulation results are provided in Section V, and conclusions are drawn in Section VI.

## II. SYSTEM MODEL FOR DISTRIBUTED UAV PLATFORMS

We first establish the system model consisting of static (or slowly moving so that the Doppler effect can be ignored) targets and UAV platforms, and the dynamic case of moving targets and UAV platforms will be introduced in Section IV.

Consider a distributed sensor array network with  $M$  sub-arrays and each sub-array is fixed on a UAV platform, where  $U_m(x_m, y_m)$  represents the location of the  $m$ -th UAV in a predefined Cartesian coordinate system as shown in Fig. 1. For this distributed sensor array network, a transmitter is employed to send relatively narrowband (compared to the sub-array

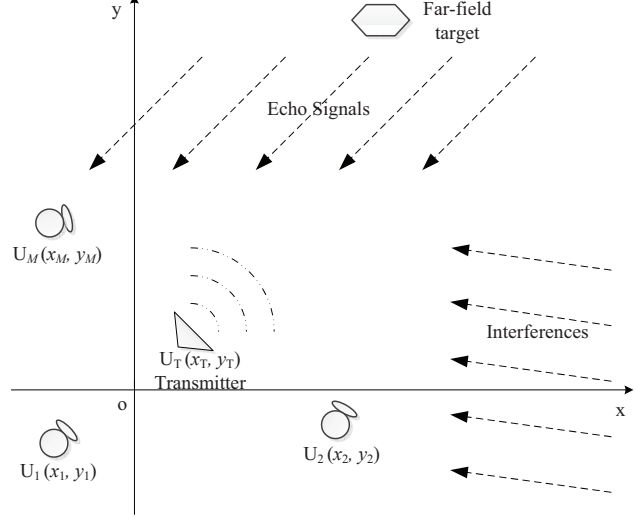


Fig. 1. A general model for a distributed sensor array system based on UAV platforms.

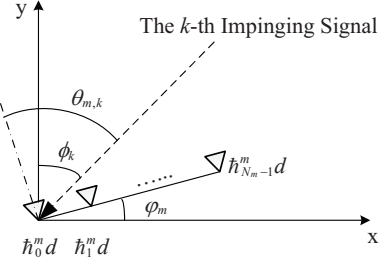


Fig. 2. A general array structure for the  $m$ -th UAV.

aperture) electro-magnetic waves into the space, and the echo signals reflected from far-field targets are then received by the sub-array placed on each UAV. There are also interferences impinging on each sub-array from unknown directions.

Without loss of generality, the structure of an  $L_m$ -sensor linear sub-array on the  $m$ -th UAV is shown in Fig. 2. Assume that there are  $K$  narrowband signals  $s_{m,k}(t)$  (including the echo signals and interferences) observed at the  $m$ -th sub-array, impinging from incident angles  $\phi_k$ ,  $k = 1, 2, \dots, K$ , in the Cartesian coordinate system, where  $\phi_k$  is measured between the direction of the signal and the  $y$ -axis.  $\varphi_m$  is an arbitrary rotation angle for the  $m$ -th UAV which is measured between the end-fire direction of the linear sub-array and the  $x$ -axis, while  $\theta_{m,k}$  represents the incident angle of the  $k$ -th signal based on the sub-array, which is defined between the direction of the signal and the broadside of the array. Clearly,  $\theta_{m,k} = \phi_k + \varphi_m$ , and the sensor position set  $\mathbb{S}_m$  is given as

$$\mathbb{S}_m = \{h_l^m d, 0 \leq l_m \leq L_m - 1, l_m \in \mathbb{Z}\}, \quad (1)$$

where  $\mathbb{Z}$  is the set of all integers, and  $d$  is the unit spacing satisfying  $d \leq \lambda/2$  with  $\lambda$  being the signal wavelength.

We use  $\mathbf{x}_m(t)$  to represent the  $L_M \times 1$  array observed signal vector, and the narrowband array output model is given by

$$\mathbf{x}_m(t) = \mathbf{A}(\theta_m, t)\mathbf{s}_m(t) + \bar{\mathbf{n}}_m(t), \quad (2)$$

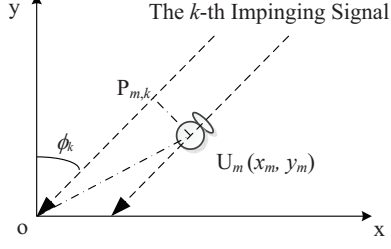


Fig. 3. The time delay.

where  $\mathbf{s}_m(t) = [s_{m,1}(t), s_{m,2}(t), \dots, s_{m,K}(t)]^T$  is the signal vector consisting of all the impinging signals, and  $\{\cdot\}^T$  denotes the transpose operation.  $\bar{\mathbf{n}}_m(t)$  represents the noise vector of the  $m$ -th sub-array carried by the corresponding UAV, and the  $L_m \times K$  steering matrix  $\mathbf{A}(\theta_m, t) = [\mathbf{a}(\theta_{m,1}, t), \dots, \mathbf{a}(\theta_{m,K}, t)]$ , with its  $k$ -th column vector  $\mathbf{a}(\theta_{m,k}, t)$  being the steering vector corresponding to the  $k$ -th source signal, expressed as

$$\mathbf{a}(\theta_{m,k}, t) = [a_{0,k}^m(t), a_{1,k}^m(t), \dots, a_{L_m-1,k}^m(t)]^T, \quad (3)$$

with

$$a_{l_m,k}^m(t) = b_{l_m,k}^m(t)e^{-j\frac{2\pi h_{l_m}^m d}{\lambda} \sin(\theta_{m,k})}, \quad (4)$$

where  $b_{l_m,k}^m(t)$  is the reflection coefficient of the target corresponding to the  $l_m$ -th sensor of the  $m$ -th sub-array, and may be time-varying due to target motion or radar cross section (RCS) fluctuations. For the observed time window,  $b_{l_m,k}^m(t)$  of the far-field target can be assumed to be nearly unchanged.

The time delay between different sub-arrays reflects the difference of the observed signals for sensors located at different sub-arrays. Since the spacing between sub-arrays is much larger than the signal wavelength, the difference between those received signals across sub-arrays can not be considered as a phase shift any more, although the signal itself is narrowband. As shown in Fig. 3, taking the origin O(0,0) as the reference, the angle  $\angle XOU_m$  between the x-axis and the direction from the origin to the point  $U_m(x_m, y_m)$  can be obtained by

$$\begin{aligned} \angle XOU_m &= \arctan 2(y_m, x_m) \\ &= \begin{cases} \arctan(\frac{y_m}{x_m}), & x_m > 0, \\ \arctan(\frac{y_m}{x_m}) + \pi, & y_m \geq 0, x_m < 0, \\ \arctan(\frac{y_m}{x_m}) - \pi, & y_m < 0, x_m < 0, \\ +\frac{\pi}{2}, & y_m > 0, x_m = 0, \\ -\frac{\pi}{2}, & y_m < 0, x_m = 0, \\ \text{undefined}, & y_m = 0, x_m = 0, \end{cases} \end{aligned} \quad (5)$$

where  $\arctan 2(y_m, x_m) \in (-\pi, \pi]$  returns the four-quadrant inverse tangent of  $y_m$  and  $x_m$ , while  $\arctan(\frac{y_m}{x_m})$  returns the inverse tangent of  $\frac{y_m}{x_m}$ .

Denote  $R_{AB}$  as the distance between positions A and B. Then, we have  $R_{OU_m} = \sqrt{x_m^2 + y_m^2}$  and  $\angle P_{m,k}OU_m = \frac{\pi}{2} - \angle XOU_m + \phi_k$ . Therefore, we can obtain  $R_{OP_{m,k}} = R_{OU_m} \cos(\angle P_{m,k}OU_m)$ , and the time delay of the  $m$ -th UAV at  $U_m$  is

$$\Delta\tau_{m,k} = -\frac{R_{OP_{m,k}}}{c} = -\frac{\sqrt{x_m^2 + y_m^2} \cdot \cos(\angle P_{m,k}OU_m)}{c}, \quad (6)$$

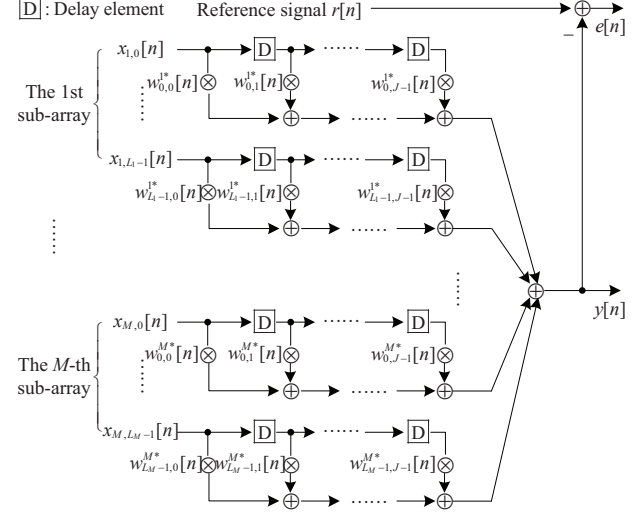


Fig. 4. A general structure of the proposed joint reference signal based beamformer.

where  $c$  is the wave propagation speed.

We stack  $\Delta\tau_{m,k}$  for the  $m$ -th UAV into a vector as  $\boldsymbol{\tau}_m = [\Delta\tau_{m,1}, \Delta\tau_{m,2}, \dots, \Delta\tau_{m,K}]^T$ , and the signal observed at the origin O(0,0) is denoted as  $\tilde{s}_k(t) = s_k(t)e^{j2\pi f_c t}$ ,  $k = 1, 2, \dots, K$ , where  $f_c$  is the carrier frequency and  $s_k(t)$  is the baseband signal. Note that  $\tilde{s}_k(t)$  is a delayed copy of the transmitted signal if the  $k$ -th impinging signal is the echo signal reflected back from a target. Then, the array output model of the  $m$ -th sub-array is updated to

$$\begin{aligned} \mathbf{x}_m(t) &= \mathbf{A}(\theta_m, t)\mathbf{s}_m(t) + \bar{\mathbf{n}}_m(t) \\ &= \mathbf{A}(\theta_m, t)\mathbf{s}(t - \boldsymbol{\tau}_m) + \bar{\mathbf{n}}_m(t), \end{aligned} \quad (7)$$

where the signal vector for the  $m$ -th UAV is  $\mathbf{s}(t - \boldsymbol{\tau}_m) = [\tilde{s}_1(t - \Delta\tau_{m,1}), \tilde{s}_2(t - \Delta\tau_{m,2}), \dots, \tilde{s}_K(t - \Delta\tau_{m,K})]^T$ .

### III. JOINT REFERENCE SIGNAL BASED BEAMFORMER FOR DISTRIBUTED SENSOR ARRAY NETWORK

#### A. The Structure of the Proposed Beamformer for Static/Slowly Moving Targets and UAV Platforms

To exploit the information acquired by all sub-arrays simultaneously, we propose a novel joint reference signal based beamformer (JRSB), and its structure after down conversion to remove the carrier frequency  $f_c$  and analogue to digital conversion (ADC) with a sampling frequency  $f_s$  is given in Fig. 4, where  $J-1$  delay elements are allocated for each sensor channel and  $T_s = 1/f_s$  is the delay between adjacent taps of the tapped delay-lines (TDLs), which are actually equivalent to a series of finite impulse response (FIR) filters.  $x_{m,l}[n]$  is the signal received at the  $l$ -th sensor of the  $m$ -th sub-array,  $r[n]$  is the reference signal considered as a properly delayed copy of the known transmitted signal, the weight vector  $\mathbf{w}_m[n] = [\{\mathbf{w}_0^m[n]\}^T, \{\mathbf{w}_1^m[n]\}^T, \dots, \{\mathbf{w}_{J-1}^m[n]\}^T]^T$  holds  $L_m J$  complex coefficients, with each  $\mathbf{w}_j^m[n] = [w_{0,j}^m[n], w_{1,j}^m[n], \dots, w_{L_m-1,j}^m[n]]^T$ ,  $j = 0, 1, \dots, J-1$ , and  $\{\cdot\}^*$  denotes the complex conjugate operation.

Construct an  $LJ \times 1$  weight vector  $\mathbf{w}[n] = [\mathbf{w}_1^T[n], \mathbf{w}_2^T[n], \dots, \mathbf{w}_M^T[n]]^T$  with  $L = \sum_{m=1}^M L_m$ , and a large  $LmJ \times 1$  observed signal vector by  $\tilde{\mathbf{x}}_m[n] = [\mathbf{x}_m^T[n], \mathbf{x}_m^T[n-1], \dots, \mathbf{x}_m^T[n-(J-1)]]^T$ .

Then, the observed signal vector is further extended to the size of  $LJ \times 1$  by  $\tilde{\mathbf{x}}[n] = [\tilde{\mathbf{x}}_1^T[n], \tilde{\mathbf{x}}_2^T[n], \dots, \tilde{\mathbf{x}}_M^T[n]]^T$ . As a result, the output  $y[n]$  is

$$y[n] = \mathbf{w}^H[n]\tilde{\mathbf{x}}[n], \quad (8)$$

with  $\{\cdot\}^T$  denoting the Hermitian transpose. The error between the reference signal  $r[n]$  and the beamformer output  $y[n]$  is obtained by

$$\begin{aligned} e[n] &= r[n] - y[n] \\ &= r[n] - \mathbf{w}^H[n]\tilde{\mathbf{x}}[n]. \end{aligned} \quad (9)$$

### B. Adaptive Algorithms for the Proposed Beamformer

Based on our proposed structure, we can construct a reference signal based beamformer employing all kinds of standard adaptive filtering algorithms, such as the least mean square (LMS) algorithm and the recursive least squares (RLS) algorithm [4]. As representative examples, the Wiener solution based on finite sample approximation and the normalized least mean square algorithm (NLMS), a stochastic gradient based algorithm, are employed for beamforming in this paper. The cost function  $\xi[n]$  at the time instant  $n$ , which is constructed by the mean square error (MSE), can be formulated as

$$\begin{aligned} \xi[n] &= E\{e[n]e^*[n]\} \\ &= E\{(r[n] - \mathbf{w}^H[n]\tilde{\mathbf{x}}[n])(r[n] - \mathbf{w}^H[n]\tilde{\mathbf{x}}[n])^*\} \\ &= \sigma_r^2 - \mathbf{w}^H[n]\mathbf{p} - \mathbf{p}^H\mathbf{w}[n] + \mathbf{w}^H[n]\mathbf{R}_{\mathbf{xx}}\mathbf{w}[n], \end{aligned} \quad (10)$$

where  $E\{\cdot\}$  is the expectation operation,  $\sigma_r^2 = E\{r[n]r^*[n]\}$ ,  $\mathbf{p} = E\{\tilde{\mathbf{x}}[n]r^*[n]\}$  is the cross-correlation vector between the reference signal and the received array signals, and  $\mathbf{R}_{\mathbf{xx}} = E\{\tilde{\mathbf{x}}[n]\tilde{\mathbf{x}}^H[n]\}$  is the covariance matrix of the received signals.

The gradient vector of the above cost function  $\xi[n]$  with respect to  $\mathbf{w}^H[n]$  can be evaluated as

$$\nabla\xi[n] = -\mathbf{p} + \mathbf{R}_{\mathbf{xx}}\mathbf{w}[n]. \quad (11)$$

By setting the above gradient vector to zero, we obtain the optimum weight vector  $\mathbf{w}_{\text{opt}}$  giving the minimum MSE value, i.e., the so-called Wiener solution [4], [13]

$$\mathbf{w}_{\text{opt}} = \mathbf{R}_{\mathbf{xx}}^{-1}\mathbf{p}. \quad (12)$$

In practice, it is impossible to obtain the covariance matrix  $\mathbf{R}_{\mathbf{xx}}$  and the cross-correlation vector  $\mathbf{p}$  of the received signals exactly, and we have to estimate them from the available data samples. In that case, we can use the following sample covariance matrix  $\tilde{\mathbf{R}}_{\mathbf{xx}}$  and sample cross-correlation vector  $\tilde{\mathbf{p}}$  to replace them, leading to the sample matrix inversion (SMI) solution based on finite sample approximation, given by

$$\mathbf{w}_{\text{SMI}} = \tilde{\mathbf{w}}_{\text{opt}} = \tilde{\mathbf{R}}_{\mathbf{xx}}^{-1}\tilde{\mathbf{p}}. \quad (13)$$

where

$$\begin{aligned} \tilde{\mathbf{R}}_{\mathbf{xx}} &= \frac{1}{N} \sum_{n=0}^{N-1} \tilde{\mathbf{x}}[n]\tilde{\mathbf{x}}^H[n], \\ \tilde{\mathbf{p}} &= \frac{1}{N} \sum_{n=0}^{N-1} \tilde{\mathbf{x}}[n]r^*[n], \end{aligned} \quad (14)$$

with  $N$  being the number of data samples received.

However, a sufficient number of samples is required for accurate second-order statistics approximation, and its complexity is extremely high due to the inverse operation, especially for  $\tilde{\mathbf{R}}_{\mathbf{xx}}$  with large dimensions.

A low-complexity alternative is to update the weight vector with each new data sample coming in. By simply replacing each of the expectation values via an instantaneous single sample estimate based on the input vector  $\tilde{\mathbf{x}}[n]$  and the reference signal  $r[n]$ , given by  $\hat{\mathbf{p}} = \tilde{\mathbf{x}}[n]r^*[n]$  and  $\hat{\mathbf{R}}_{\mathbf{xx}} = \tilde{\mathbf{x}}[n]\tilde{\mathbf{x}}^H[n]$ , the gradient vector in (12) is approximately to

$$\nabla\xi[n] \approx -\hat{\mathbf{p}} + \hat{\mathbf{R}}_{\mathbf{xx}}\mathbf{w}[n] = -e^*[n]\tilde{\mathbf{x}}[n]. \quad (15)$$

Then, we can update the weight vector  $\mathbf{w}[n]$  in the negative direction of the gradient with a step size  $\mu_0$  as follows,

$$\mathbf{w}[n+1] = \mathbf{w}[n] + \mu_0 e^*[n]\tilde{\mathbf{x}}[n], \quad (16)$$

which leads directly to the well-known least mean square (LMS) algorithm. The factor  $\mu_0$  is a positive real-valued constant weighting the amount of innovation applied at each step.

Optimal choice of the step size is data dependent and it can be normalized to ensure an approximately constant rate of adaptation by defining

$$\mu_0 = \frac{\mu}{\tilde{\mathbf{x}}^H[n]\tilde{\mathbf{x}}[n]}. \quad (17)$$

Replacing  $\mu_0$  by  $\mu$  in (16) yields the normalized least mean square algorithm (NLMS) expressed as

$$\mathbf{w}[n+1] = \mathbf{w}[n] + \frac{\mu}{\tilde{\mathbf{x}}^H[n]\tilde{\mathbf{x}}[n]} e^*[n]\tilde{\mathbf{x}}[n]. \quad (18)$$

In practice, to ensure stability of the algorithm, we normally choose  $0 < \mu < 0.5$ .

## IV. FREQUENCY EXTENDED JOINT REFERENCE SIGNAL BASED BEAMFORMER FOR MOVING TARGETS AND UAV PLATFORMS

### A. System Model for Moving Targets and UAV Platforms

In general, the targets and the UAV platforms are moving towards different directions, as shown in Fig. 5, where  $v_T$  and  $v_{U_m}$  represent the velocity of the transmitter based platform and the  $m$ -th UAV platform, respectively, and  $v_k$  is the velocity of the  $k$ -th target. When they are moving fast enough relative to each other, the Doppler effect has to be considered. Denote  $\alpha_{T,k}$  as the angle between the moving direction of the transmitter and the opposite impinging direction of the  $k$ -th echo signal,  $\alpha_{m,k}$  is the angle measured between the moving direction of the  $m$ -th UAV and the opposite impinging direction of the  $k$ -th echo signal, while  $\alpha_k$  is the angle between

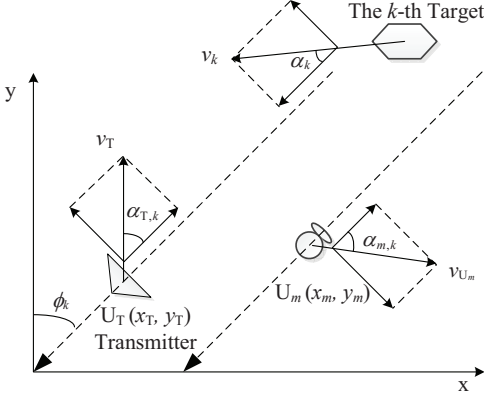


Fig. 5. The relative velocity between the target and the  $m$ -th UAV platform.

the moving direction of the  $k$ -th target and the impinging direction of its echo signal. Clearly, the radial velocity  $v_{T,k}$  between the  $k$ -th target and the transmitter, and the radial velocity  $v_{m,k}$  between the  $k$ -th target and the  $m$ -th UAV are obtained by

$$\begin{aligned} v_{T,k} &= v_T \cos \alpha_{T,k} + v_k \cos \alpha_k, \\ v_{m,k} &= v_{U_m} \cos \alpha_{m,k} + v_k \cos \alpha_k. \end{aligned} \quad (19)$$

Then, we can obtain the Doppler frequency of the  $k$ -th target received at the  $m$ -th UAV as

$$f_{m,k} = \frac{v_{T,k} + v_{m,k}}{\lambda}, \quad (20)$$

and therefore, for the moving targets and UAV platforms, the observed signal model (7) is reformulated as

$$\begin{aligned} \mathbf{x}_m(t) &= \mathbf{A}(\boldsymbol{\theta}_m, t)\mathbf{s}_m(t) + \bar{\mathbf{n}}_m(t) \\ &= \mathbf{A}(\boldsymbol{\theta}_m, t)\mathbf{s}(t - \boldsymbol{\tau}_m) + \bar{\mathbf{n}}_m(t). \end{aligned} \quad (21)$$

where the column vector  $\mathbf{s}(t - \boldsymbol{\tau}_m)$  is updated to  $\mathbf{s}(t - \boldsymbol{\tau}_m) = [\bar{s}_1(t - \Delta\tau_{m,1}), \bar{s}_2(t - \Delta\tau_{m,2}), \dots, \bar{s}_K(t - \Delta\tau_{m,K})]^T$  with  $\bar{s}_k(t) = s_k(t)e^{2\pi(f_c + f_{m,k})t}$  and  $s_k(t)$  being the baseband signal. Now the  $k$ -th impinging signal observed at the origin is changed to  $\tilde{s}_k(t) = s_k(t)e^{j2\pi(f_c + f_{0,k})t}$ ,  $k = 1, 2, \dots, K$ , with the Doppler frequency at the origin being  $f_{0,k} = \frac{v_T \cos \alpha_{T,k} + 2v_k \cos \alpha_k}{\lambda}$ .

### B. Frequency Extended Joint Reference Signal Based Beamformer

After down conversion to remove the carrier frequency  $f_c$  and ADC with  $f_s$ , the Doppler frequency is still included in the obtained signals at each sensor channel, leading to performance degradation using the proposed JRSB. To perform beamforming without prior knowledge of the motion parameters of both the targets and the UAV platforms, we propose a frequency extended joint reference signal based beamformer (FE-JRSB) to exploit the information across the frequencies of interest by modulating the received signals into different frequency bins at first. Assume that the maximum Doppler frequency is  $f_{d,\max}$ , and the frequency range of interest  $[-f_{d,\max}, f_{d,\max}]$  is divided to  $Q$  bins with the center frequency of the  $q$ -th frequency bin as

$$f_q = -f_{d,\max} + q \cdot \frac{2f_{d,\max}}{Q-1}, \quad (22)$$

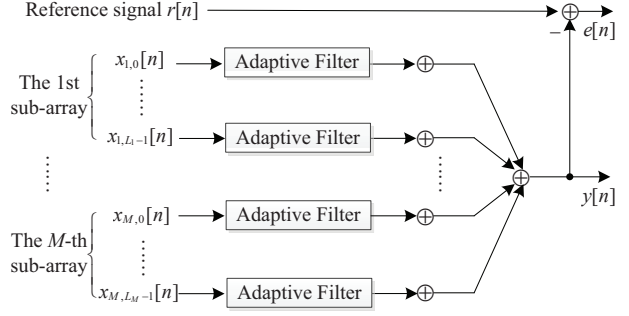


Fig. 6. A general structure for the proposed frequency extended joint reference signal based beamformer.

$\boxed{D}$ : Delay element

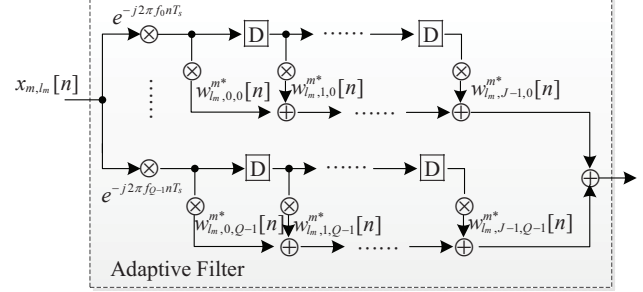


Fig. 7. A general structure of the adaptive filter for the  $l_m$ -th sensor of the  $m$ -th UAV.

where  $q = 0, 1, \dots, Q-1$ .

Fig. 6 gives the general structure of the proposed FE-JRSB, where the adaptive filter for the  $l_m$ -th sensor of the  $m$ -th UAV is shown in Fig. 7 with  $J-1$  delay elements allocated for each frequency bin at each sensor channel and  $T_s = 1/f_s$ . The column vector holding  $L_m Q$  complex coefficients is constructed by

$$\begin{aligned} \mathbf{w}_j^m[n] &= [w_{0,j,0}^m[n], w_{1,j,0}^m[n], \dots, w_{L_m-1,j,0}^m[n], \\ &\quad w_{0,j,1}^m[n], w_{1,j,1}^m[n], \dots, w_{L_m-1,j,1}^m[n], \\ &\quad \dots, \\ &\quad w_{0,j,Q-1}^m[n], w_{1,j,Q-1}^m[n], \dots, w_{L_m-1,j,Q-1}^m[n]]^T, \end{aligned} \quad (23)$$

where  $j = 0, 1, \dots, J-1$ .

Then the  $L_m J Q \times 1$  weight vector is obtained by  $\mathbf{w}_m[n] = [\{\mathbf{w}_0^m[n]\}^T, \{\mathbf{w}_1^m[n]\}^T, \dots, \{\mathbf{w}_{J-1}^m[n]\}^T]^T$ , and the  $L J Q \times 1$  weight vector is  $\mathbf{w}[n] = [\mathbf{w}_1^T[n], \mathbf{w}_2^T[n], \dots, \mathbf{w}_M^T[n]]^T$ .

Denote  $\gamma_q = e^{-j2\pi f_q n T_s}$ ,  $q = 0, 1, \dots, Q-1$ . Construct a large  $L_m J Q \times 1$  observed signal vector by

$$\begin{aligned} \tilde{\mathbf{x}}_m[n] &= [\gamma_0 \mathbf{x}_m^T[n], \dots, \gamma_{Q-1} \mathbf{x}_m^T[n], \\ &\quad \gamma_0 \mathbf{x}_m^T[n-1], \dots, \gamma_{Q-1} \mathbf{x}_m^T[n-1], \\ &\quad \dots, \\ &\quad \gamma_0 \mathbf{x}_m^T[n-(J-1)], \dots, \gamma_{Q-1} \mathbf{x}_m^T[n-(J-1)]]^T. \end{aligned} \quad (24)$$

Then, the observed signal vector is further extended to the size of  $L J \times 1$  by  $\tilde{\mathbf{x}}[n] = [\tilde{\mathbf{x}}_1^T[n], \tilde{\mathbf{x}}_2^T[n], \dots, \tilde{\mathbf{x}}_M^T[n]]^T$ . Similarly,

the output  $y[n]$  is

$$y[n] = \mathbf{w}^H[n]\tilde{\mathbf{x}}[n], \quad (25)$$

while the error between the reference signal  $r[n]$  and the FE-JRSB output  $y[n]$  is obtained by

$$\begin{aligned} e[n] &= r[n] - y[n] \\ &= r[n] - \mathbf{w}^H[n]\tilde{\mathbf{x}}[n]. \end{aligned} \quad (26)$$

Based on the proposed FE-JRSB structure, the NLMS algorithm and the SMI solution can be also employed for beamforming.

*Remarks:* The proposed FE-JRSB can also be applied to the scenario where the baseband signal is sent through multiple carrier frequencies to exploit the frequency diversity of the target's RCS fluctuations simultaneously. In that case,  $\gamma_q$  is changed to the step frequencies between the multiple carrier frequencies and the reference frequency, and this modulation part regarding  $\gamma_q$  may be implemented at the down conversion stage using different frequencies.

## V. SIMULATION RESULTS

Consider  $M = 3$  sub-arrays distributed on three UAV platforms, and each sub-array is a uniform linear array with  $L_m = 5$  sensors,  $\forall m = 1, 2, 3$ , and  $d = \lambda/2$ . The positions of the three sub-arrays are  $U_1(0, -50)$ ,  $U_2(25, 10)$ , and  $U_3(-70, 90)$ , while their rotation angles are  $45^\circ$ ,  $28^\circ$ , and  $-19^\circ$ , respectively. With a coarse estimation of the target range of interest, we adjust the reference signal with a proper time delay compared to the transmitted signal, and set  $J = 80$ , and  $\mu = 0.1$ . For the far-field targets, the reflection coefficients  $b_{l_m,k}^m(t)$  are randomly generated constant complex values sharing the same amplitude for all sensors, and the signal to noise ratio (SNR) is set to be 20dB, defined within the bandwidth of interest. The working frequency is 10 GHz and the signal propagation speed is  $3 \times 10^8$  m/s with the signal wavelength  $\lambda = 0.03$ m. The spacings among the UAV platforms are 65.00m, 124.20m, and 156.52m, respectively, and all of them are at least  $10^3$  times larger than the signal wavelength. It is noted that these information are unknown for the beamformers. In practice, all the information collected by UAVs can be sent to a base station for centralized processing.

### A. Simulation Results for Static/Slowly Moving Targets and UAV Platforms

#### 1) Simulation Results for $K = 1$

In the first scenario, there is only one far-field target with incident angle of  $\theta_1 = -10^\circ$ , i.e.,  $K = 1$ . Then, we focus on the ensemble mean square error (MSE) results of  $e[n]$  with respect to the number of samples, which is also the iteration number of the NLMS algorithm. The ensemble MSE is defined as

$$\text{EMSE}[n] = \sqrt{\frac{1}{Q} \sum_{q=1}^Q |\hat{e}_q[n]|^2}, \quad (27)$$

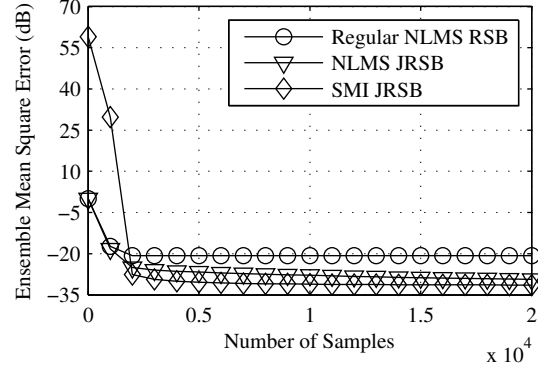


Fig. 8. Ensemble mean square error of different beamformers for  $K = 1$ .

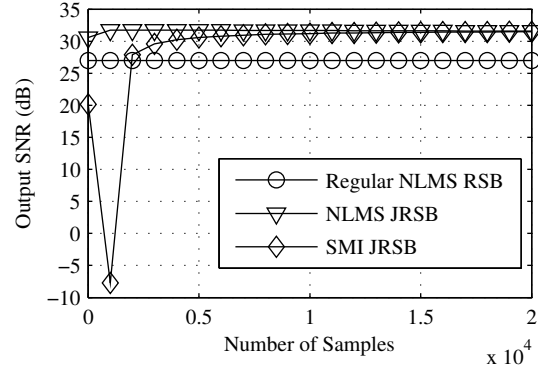


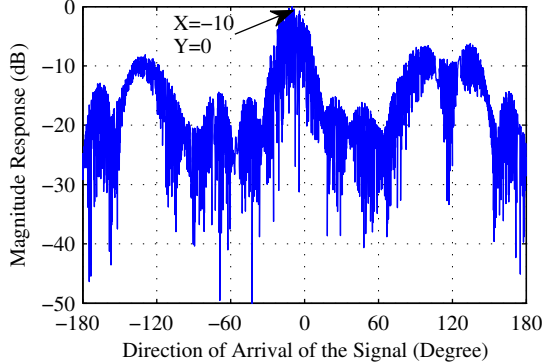
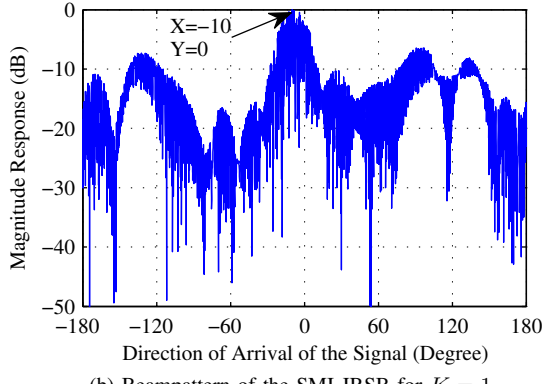
Fig. 9. Output SNR of different beamformers for  $K = 1$ .

where  $Q$  is the number of independent simulation runs, and  $\hat{e}_q[n]$  represents the error at iteration number  $n$  of the  $q$ -th trial.

The ensemble MSE results for different beamformers are shown in Fig. 8, where each point is based on an average of the results obtained by  $Q = 500$  Monte Carlo simulation runs, the regular NLMS RSB represents the reference signal based beamforming results using the NLMS algorithm based on a single sub-array located at  $U_1(0, -50)$  with a rotation angle  $45^\circ$ , the NLMS JRSB is the proposed JRSB employing the NLMS algorithm, and the SMI JRSB represents the proposed JRSB using the SMI solution. It is noted that  $\tilde{\mathbf{R}}_{xx}$  is a matrix with a size of  $1200 \times 1200$ , and there exists serious degradation in the performance of the SMI JRSB for a small number of samples less than 1000 due to worse approximations to the second-order statistics. Clearly, both the NLMS JRSB and the SMI JRSB (when the number of samples are larger than 1000) outperform the regular one, and the best performance is achieved by the SMI JRSB.

Then, the output SNR of different beamformers are shown in Fig. 9. It is obvious that the output SNR of the regular NLMS RSB is the worst among the three beamformers, while the output SNR of the NLMS JRSB and the SMI JRSB are close to each other with that of the NLMS JRSB a bit higher.

We then fix all the reflection coefficients to 1, and the beampatterns obtained by the NLMS JRSB and the SMI JRSB are shown in Fig. 10(a) and Fig. 10(b), respectively. Since the spacing between UAVs are extremely larger than the signal

(a) Beampattern of the NLMS JRSB for  $K = 1$ .(b) Beampattern of the SMI JRSB for  $K = 1$ .Fig. 10. Beampattern for  $K = 1$ .

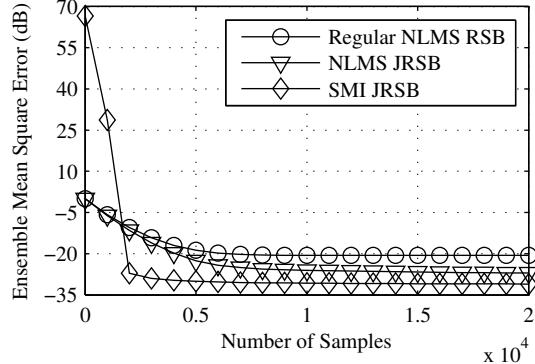
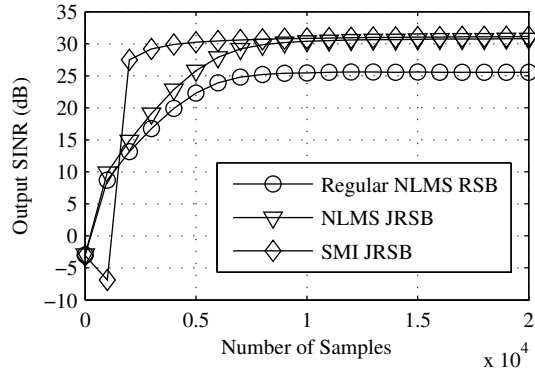
wavelength at the working frequency, the grating lobes result in rapid fluctuations in the beampattern. However, we can still see that the signal of interest is located at the DOA angle  $-10^\circ$  with a corresponding main beam.

### 2) Simulation Results for $K = 3$

In the second scenario, there are  $K = 3$  impinging signals with the echo signal  $s_1[n]$  along with its delayed ones observed at each sub-array  $s_{m,1}[n]$ ,  $m = 1, 2, \dots, M$ , being the signals of interest, while others are interferences to be suppressed. The incident angle of the echo signal is  $\theta_1 = -10^\circ$ , whereas the two interferences come from  $-30^\circ$  and  $20^\circ$ , respectively. The signal to interference ratio (SIR) for each interfering signal is 0dB, defined within the bandwidth of interest.

The ensemble MSE results for different beamformers are shown in Fig. 11. It is clear that both the NLMS JRSB and the SMI JRSB provide a much faster convergence speed as well as lower MSEs compared with the regular one. Furthermore, the SMI JRSB provides the best results for a sufficient number of samples involved in the second-order statistics approximation, but with a high computational complexity. Similar to the first scenario, there is serious degradation in the performance of the SMI JRSB when the number of samples is less than 1000.

Fig. 12 gives the output signal to interference plus noise ratio (SINR) of different beamformers, which is consistent with the ensemble MSE results in Fig. 11, and an improved output SINR has been achieved by both JRSBs compared to the regular NLMS RSB, with the SMI JRSB being the best.

Fig. 11. Ensemble mean square error of different beamformers for  $K = 3$ .Fig. 12. Output SINR of different beamformers for  $K = 3$ .

Then, we give the beampatterns of the proposed NLMS JRSB and the SMI JRSB by fixing all the reflection coefficients to be 1, as shown in Fig. 13(a) and Fig. 13(b), respectively. Clearly, the signal of interest at incident angle  $-10^\circ$  is enhanced while interferences at DOAs of  $-30^\circ$  and  $20^\circ$  are suppressed.

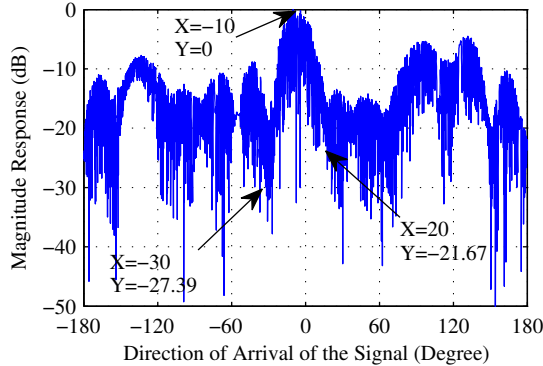
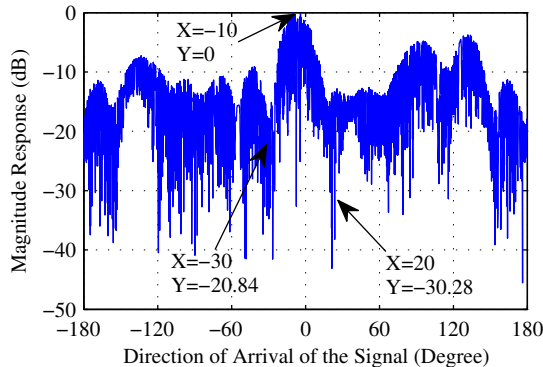
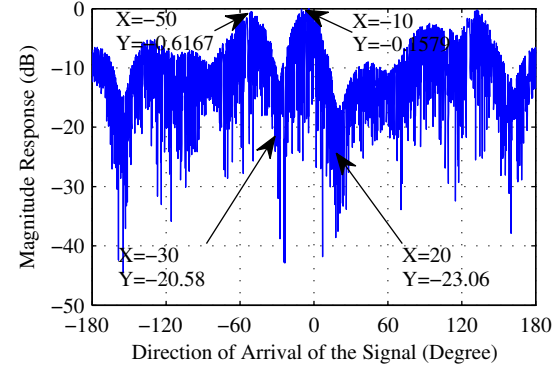
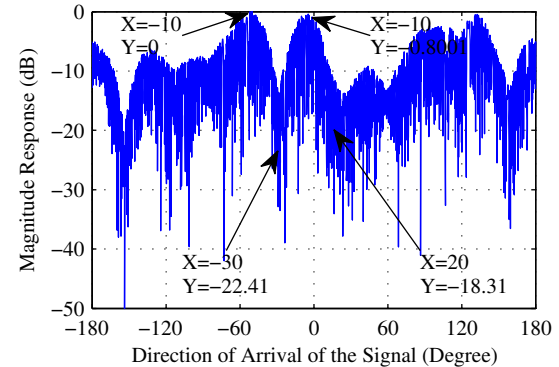
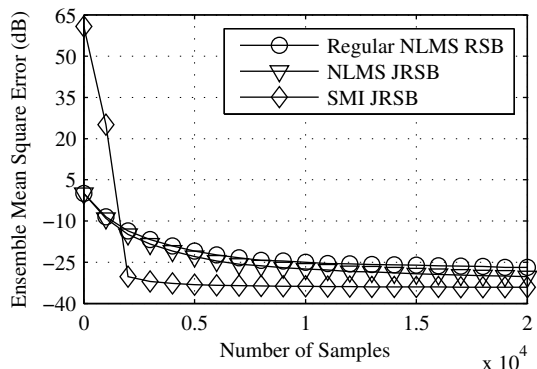
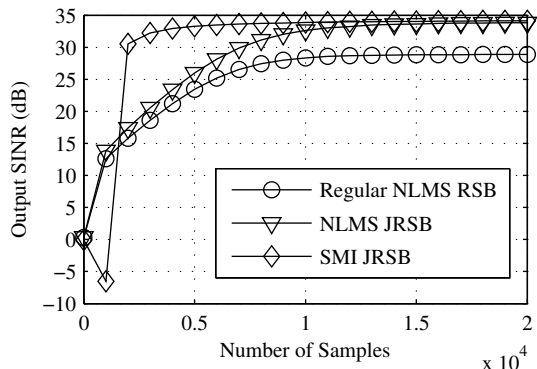
### 3) Simulation Results for $K = 4$

To further study the performance of different beamformers, another far-field target with incident angle of  $-50^\circ$  is added compared to the second scenario, and now there are four impinging signals with two being of interest. The ensemble MSE results and the output SINR of different beamformers are shown in Figs. 14 and 15, respectively, which again verify the superior performance of the proposed NLMS JRSB and SMI JRSB.

Finally, we fix all the reflection coefficients to 1, and the beampatterns of the proposed NLMS JRSB and the SMI JRSB for two targets are shown in Fig. 16(a) and Fig. 16(b), respectively. We can see clearly that the two signals of interest at incident angles  $-50^\circ$  and  $-10^\circ$  are enhanced, whereas the two interferences at DOAs of  $-30^\circ$  and  $20^\circ$  are suppressed.

### 4) Detection Probability

From Figs. 9 and 12, we can see that the output SNR or SINR of the JRSBs for a large number of samples is around 4.5dB higher than that of the regular NLMS RSB, which is close to the gain brought by the three sub-arrays with  $10 \log_{10} 3 = 4.8$ dB. Furthermore, as indicated in Fig. 15, the

(a) Beampattern of the NLMS JRSB for  $K = 3$ .(b) Beampattern of the SMI JRSB for  $K = 3$ .Fig. 13. Beampatterns for  $K = 3$ .(a) Beampattern of the NLMS JRSB for  $K = 4$  with two targets.(b) Beampatterns for  $K = 4$  with two targets.Fig. 16. Beampatterns for  $K = 4$  with two targets.Fig. 14. Ensemble mean square error of different beamformers for  $K = 4$  with two targets.Fig. 15. Output SINR of different beamformers for  $K = 4$  with two targets.

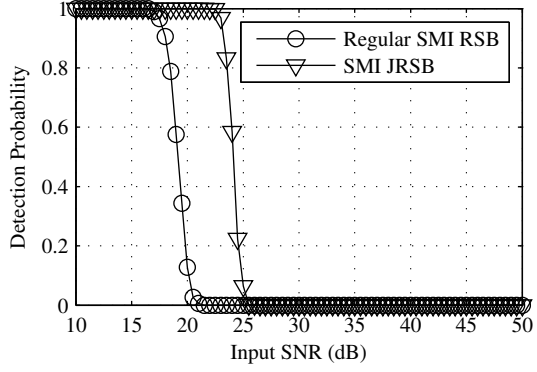
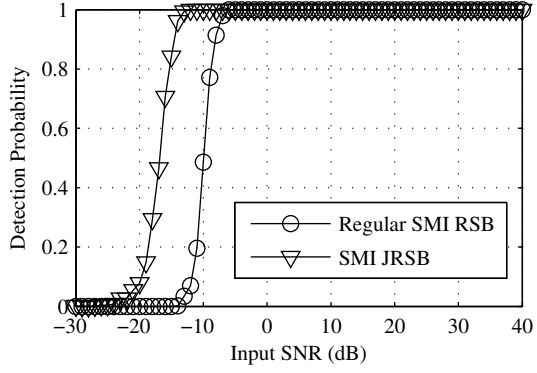
output SINR with two targets of interest is nearly 3dB higher than the other two scenarios with only one target of interest. As a result, the proposed JRSB is capable of performing coherent addition across all sub-arrays and targets, achieving a maximum output SINR for target detection.

To compare the detection probability of the proposed beamformer, we consider the second scenario as a representative example. The linear frequency modulated (LFM) signal is chosen as the transmitted signal, where the bandwidth of the LFM signal is 10MHz, the modulation period (pulse width) is 5us, and the pulse repetition time (PRT) is 25us. Other settings remain the same as in the second scenario with  $K = 3$ . Based on the beamformer output, pulse compression followed by a constant false alarm rate (CFAR) detector is applied. The detection probability of different beamformers are shown in Fig. 17. Clearly, the SMI JRSB consistently outperforms the regular SMI JRSB (JRSB based SMI solution) due to the higher output SINR. The NLMS JRSB has a very similar performance to the SMI JRSB and is not shown there.

## B. Simulation Results for Moving Targets and UAV Platforms

### 1) Simulation Results for $K = 3$

Assume that the maximum potential radial velocity between the target and the UAV platform is 30m/s, corresponding to the Doppler frequency of  $f_{d\max} = 2000\text{Hz}$  with  $\lambda = 0.03\text{m}$ . In the proposed FE-JRSB, the frequency range of interest  $[-f_{d\max}, f_{d\max}]$  is divided into 5 frequency bins with  $f_q =$

(a) Detection probability versus threshold for  $\text{SNR} = -5\text{dB}$ .(b) Detection probability versus SNR for threshold =  $15\text{dB}$ .Fig. 17. Detection probability of different beamformers for  $K = 3$ .

$-2000 + 1000q$ ,  $q = 0, 1, \dots, 4$ . In the first scenario, we set  $K = 3$  with one signal of interest and two interferences, and the incident angle of the echo signal is  $\theta_1 = -10^\circ$ , whereas the two interferences come from  $-30^\circ$  and  $20^\circ$ , respectively. The radial velocities between the moving target and each of the three UAV platforms, i.e.,  $U_1(0, -50)$  with rotation angle  $45^\circ$ ,  $U_2(25, 10)$  with rotation angle  $28^\circ$ , and  $U_3(-70, 90)$  with rotation angle  $-19^\circ$ , are  $-30\text{m/s}$ ,  $0\text{m/s}$ , and  $15\text{m/s}$ , respectively. Please note that these information are unknown to the beamformers except for the maximum potential radial velocity. The ensemble mean square error (MSE) results of  $e[n]$  with respect to the number of samples employing the SMI solution is shown in Fig. 18. Obviously, the convergence speed of the FE-JRSB is smaller than that of the JRSB, however, its MSE after adaption is lower than the other one.

Then, the output SINR of the proposed FE-JRSB and the JRSB are shown in Fig. 19. Consistent with the ensemble MSE results in Fig. 18, we can see clearly that the FE-JRSB outperforms the JRSB after adaption, and the information across the frequencies of interest collected by all the sub-array channels are exploited jointly.

## 2) Simulation Results for $K = 4$

In the second scenario for the dynamic case, another target with incident angle of  $-50^\circ$  is added based on the first scenario, and its relative radial velocities towards the three UAV platforms are set to be  $-15\text{m/s}$ ,  $15\text{m/s}$ , and  $30\text{m/s}$ , respectively.

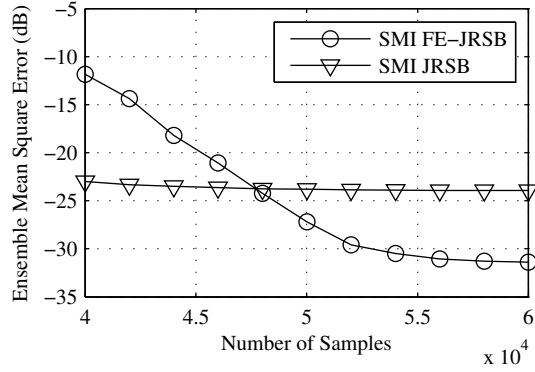
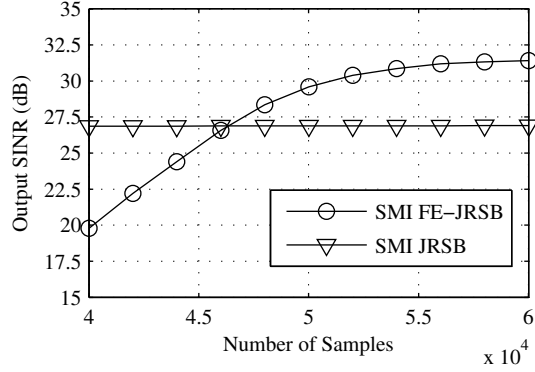
Fig. 18. Ensemble mean square error results of different beamformers for  $K = 3$  with one moving target.Fig. 19. The output SINR of different beamformers for  $K = 3$  with one moving target.

Fig. 20 shows the ensemble MSE results versus the number of samples, while Fig. 21 gives the output SINR of the two proposed beamformers, which again verifies that the FE-JRSB is capable of exploiting possible information involved in all frequency bins, leading to improved performance compared to the JRSB after adaption. Furthermore, the output SINR of the FE-JRSB is approximately 3dB higher than the achieved SINR in the first scenario, which is caused by performing coherent accumulation adaptively across all sub-arrays, frequencies of interest, and targets, and therefore a maximum output SINR for target detection is achieved by the proposed FE-JRSB for moving targets and UAV platforms without sacrificing any information.

## VI. CONCLUSIONS

In this paper, a distributed sensor array network for target detection and surveillance consisting of sub-arrays with arbitrary locations and rotation angles placed on UAV platforms has been studied, where a transmitter is used to send out a single signal while the echo signals reflected from far-field targets are then received by the distributed sensor array system. Two cases were investigated: one is for static or slowly moving targets and UAV platforms, where the Doppler effect can be ignored, while the other one is for moving targets and UAV platforms where the Doppler effect is considered. To enhance the signals of interest while suppressing interferences for the

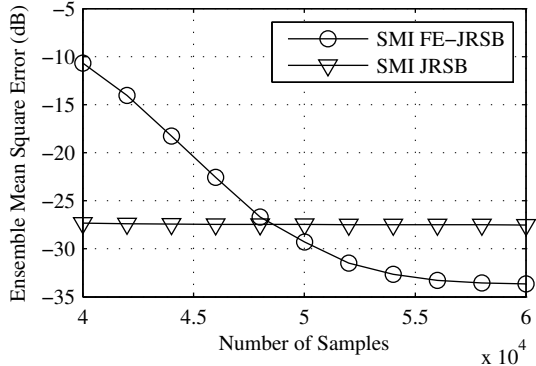


Fig. 20. Ensemble mean square error results of different beamformers for  $K = 4$  with two moving targets.

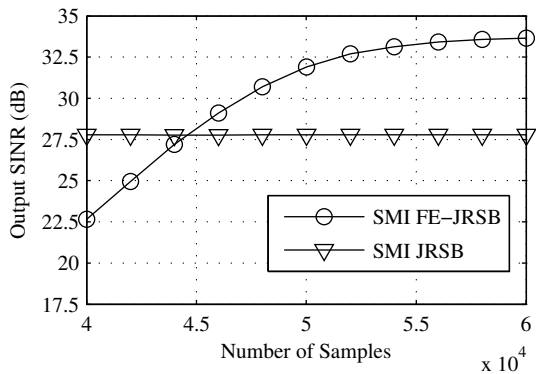


Fig. 21. The output SINR of different beamformers for  $K = 4$  with two moving targets.

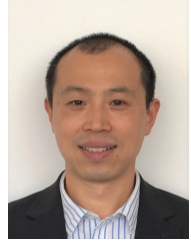
first case, a joint reference signal based beamformer (JRSB) was proposed to exploit all the collected information across different sub-arrays, where the standard NLMS algorithm and Wiener solution based on finite sample approximation are employed for adaptive beamforming. For the case with moving targets and UAV platforms, a frequency extended joint reference signal based beamformer (FE-JRSB), capable of extracting all the information across frequencies of interest, was then derived. It has been shown by simulations that the developed JRSB can work effectively and offer a much better performance than the regular beamformer applied to a single sub-array, and further improved performance is achieved by the proposed FE-JRSB for the dynamic case compared with the JRSB.

## REFERENCES

- [1] H. Krim and M. Viberg, "Two decades of array signal processing research: the parametric approach," *IEEE Signal Processing Magazine*, vol. 13, no. 4, pp. 67–94, July 1996.
- [2] L. C. Godara, "Application of antenna arrays to mobile communications, part ii: Beam-forming and direction-of-arrival estimation," *Proceedings of the IEEE*, vol. 85, no. 8, pp. 1195–1245, August 1997.
- [3] B. Allen and M. Ghavami, *Adaptive Array Systems, Fundamentals and Applications*. Chichester, England: John Wiley & Sons, 2005.
- [4] W. Liu and S. Weiss, *Wideband Beamforming: Concepts and Techniques*. Chichester, UK: John Wiley & Sons, 2010.
- [5] J. Capon, "High-resolution frequency-wavenumber spectrum analysis," *Proc. IEEE*, vol. 57, no. 8, pp. 1408–1418, Aug. 1969.
- [6] B. D. Van Veen and K. M. Buckley, "Beamforming: a versatile approach to spatial filtering," *IEEE Acoustics, Speech, and Signal Processing Magazine*, vol. 5, no. 2, pp. 4–24, April 1988.
- [7] B. Breed and J. Strauss, "A short proof of the equivalence of lcmv and gsc beamforming," *IEEE Signal Processing Letters*, vol. 9, pp. 168–169, June 2002.
- [8] R. C. de Lamare and R. Sampayo-Neto, "Low-complexity variable step-size mechanisms for stochastic gradient algorithms in minimum variance cdma receivers," *IEEE Trans. Signal Process.*, vol. 54, no. 6, pp. 2302–2317, 2006.
- [9] R. C. de Lamare, L. Wang, and R. Fa, "Adaptive reduced-rank lcmv beamforming algorithms based on joint iterative optimization of filters: Design and analysis," *Signal Processing*, vol. 90, no. 2, pp. 640–652, 2010.
- [10] J. Xu, G. Liao, S. Zhu, and L. Huang, "Response vector constrained robust lcmv beamforming based on semidefinite programming," *IEEE Trans. Signal Process.*, vol. 63, no. 21, pp. 5720–5732, 2015.
- [11] L. Zhang, W. Liu, and R. J. Langley, "A class of constrained adaptive beamforming algorithms based on uniform linear arrays," *IEEE Transactions on Signal Processing*, vol. 58, no. 7, pp. 3916–3922, July 2010.
- [12] L. Zhang, W. Liu, A. ul Quddus, M. Dianati, and R. Tafazolli, "Adaptive distributed beamforming for relay networks based on local channel state information," *IEEE Transactions on Signal and Information Processing over Networks*, vol. 1, no. 2, pp. 117–128, 2015.
- [13] S. Haykin, *Adaptive Filter Theory*, 3rd ed. Englewood Cliffs, New York: Prentice Hall, 1996.
- [14] W. Liu and S. Weiss, "Design of frequency invariant beamformers for broadband arrays," *IEEE Transactions on Signal Processing*, vol. 56, no. 2, pp. 855–860, February 2008.
- [15] Y. Zhao, W. Liu, and R. J. Langley, "Adaptive wideband beamforming with frequency invariance constraints," *IEEE Transactions on Antennas and Propagation*, vol. 59, no. 4, pp. 1175–1184, April 2011.
- [16] M. B. Hawes and W. Liu, "Sparse array design for wideband beamforming with reduced complexity in tapped delay-lines," *IEEE/ACM Trans. Audio, Speech, Language Process.*, vol. 22, no. 8, pp. 1236–1247, Aug. 2014.
- [17] Y. Bao and H. Chen, "Design of robust broadband beamformers using worst-case performance optimization: A semidefinite programming approach," *IEEE/ACM Trans. Audio, Speech, Language Process.*, vol. 25, no. 4, pp. 895–907, Apr. 2017.
- [18] M. R. Anbiyaei, W. Liu, and D. C. McLernon, "Performance improvement for wideband beamforming with white noise reduction based on sparse arrays," in *Proc. European Signal Processing Conference (EUSIPCO)*, 2017, pp. 2433–2437.
- [19] L. E. Brennan and L. Reed, "Theory of adaptive radar," *IEEE Trans. Aerosp. Electron. Syst.*, no. 2, pp. 237–252, 1973.
- [20] G. Babur, G. O. Manokhin, A. A. Geltser, and A. A. Shibelgut, "Low-cost digital beamforming on receive in phased array radar," *IEEE Trans. Aerosp. Electron. Syst.*, vol. 53, no. 3, pp. 1355–1364, 2017.
- [21] W. L. Melvin, "A STAP overview," *IEEE Aerosp. Electron. Syst. Mag.*, vol. 19, no. 1, pp. 19–35, 2004.
- [22] P. Wang, H. Li, and B. Himed, "A simplified parametric GLRT for STAP detection," in *Proc. IEEE Radar Conference*, 2009, pp. 1–5.
- [23] J. Xu, C. Wang, G. Liao, and Y. Zhang, "Sum and difference beamforming for angle-doppler estimation with stap-based radars," *IEEE Trans. Aerosp. Electron. Syst.*, vol. 52, no. 6, pp. 2825–2837, 2016.
- [24] K. Imoto and N. Ono, "Spatial cepstrum as a spatial feature using a distributed microphone array for acoustic scene analysis," *IEEE/ACM Trans. Audio, Speech, Language Process.*, vol. 25, no. 6, pp. 1335–1343, 2017.
- [25] X. Zhang, H. Li, and B. Himed, "Multistatic passive detection with parametric modeling of the io waveform," *Signal Processing*, vol. 141, pp. 187–198, 2017.
- [26] A. A. Gorji, R. Tharmarasa, and T. Kirubarajan, "Widely separated MIMO versus multistatic radars for target localization and tracking," *IEEE Trans. Aerosp. Electron. Syst.*, vol. 49, no. 4, pp. 2179–2194, 2013.
- [27] A. M. Haimovich, R. S. Blum, and L. J. Cimini, "MIMO radar with widely separated antennas," *IEEE Signal Process. Mag.*, vol. 25, no. 1, pp. 116–129, 2008.



**Qing Shen** received his B.S. degree in 2009 and Ph.D. degree in 2016, both from Beijing Institute of Technology, Beijing, China. From 2013 to 2015, He was a visiting researcher in the Department of Electronic and Electrical Engineering, University of Sheffield, Sheffield, UK. He received the Excellent Ph.D. Thesis Awards from both the Chinese Institute of Electronics and Beijing Institute of Technology in 2016. His research interests include radar and array signal processing.



**Wei Liu** (S'01-M'04-SM'10) received his BSc and LLB degrees from Peking University, China, in 1996 and 1997, respectively, MPhil from the University of Hong Kong in 2001, and PhD from the School of Electronics and Computer Science, University of Southampton, UK, in 2003. He then worked as a postdoc first at Southampton and later at the Department of Electrical and Electronic Engineering, Imperial College London. Since September 2005, he has been with the Department of Electronic and Electrical Engineering, University of Sheffield, UK,

first as a Lecturer and then a Senior Lecturer. He has published more than 250 journal and conference papers, three book chapters, and a research monograph about wideband beamforming "Wideband Beamforming: Concepts and Techniques" (John Wiley, March 2010). His research interests include sensor array signal processing, blind signal processing, multirate signal processing, and their various applications in wireless communications, radar, sonar, satellite navigation, human computer interface, and renewable energy exploitation.

He is a member of the Digital Signal Processing Technical Committee of the IEEE Circuits and Systems Society and the Sensor Array and Multichannel Signal Processing Technical Committee of the IEEE Signal Processing Society (Vice-Chair from 2019). He is currently an Associate Editor for IEEE Trans. on Signal Processing and IEEE Access, and an editorial board member of the Journal Frontiers of Information Technology and Electronic Engineering.



**Li Wang** received his B.Sc. and M.Sc. degrees in Electronic and Electrical Engineering from the University of Electronic Science and Technology of China, Chengdu, China, in 2000 and 2008, respectively. He is currently pursuing his Ph.D. degree in Sichuan University, Chengdu, China. He is the director of the Key Laboratory, the 10th Research Institute of China Electronics Technology Group Corporation. His research interests include distributed array signal processing and adaptive signal processing.



**Yin Liu** received his B.Sc., M.Sc. and Ph.D. degrees in electronic engineering from Xidian University, Xian, China, in 2002, 2005 and 2012, respectively. He is a researcher at the 10th Research Institute of China Electronics Technology Group Corporation. He is now a visiting researcher at the University of Sheffield sponsored by the China Scholarship Council. His research interests include array signal processing, sparse signal recovery, and MIMO radar signal processing.